Transport phenomena in a biomass plancha-type cookstove: Experimental performance and numerical simulations

Article *in* Energy for Sustainable Development · September 2022

DOI: 10.1016/j.esd.2022.09.019

CITATION
1

READS
151

4 authors:

Paulo Medina
Tecnologico de Estudios Superiores de Ecatepec
10 PUBLICATIONS **87** CITATIONS
SEE PROFILE

Alberto Beltran
Universidad Nacional Autónoma de México
28 PUBLICATIONS **155** CITATIONS
SEE PROFILE

Jose Nunez
Universidad Nacional Autónoma de México
33 PUBLICATIONS **111** CITATIONS
SEE PROFILE

Victor Ruiz
CONACYT and Instituto de Investigaciones en Ecosistemas y Sustentabilidad
20 PUBLICATIONS **237** CITATIONS
SEE PROFILE

Energy for Sustainable Development 71 (2022) 132–140

Contents lists available at ScienceDirect

Energy for Sustainable Development

Transport phenomena in a biomass plancha-type cookstove: Experimental performance and numerical simulations

Paulo Medina [a,b,1], Alberto Beltrán [b,*], José Núñez [c], Víctor M. Ruiz-García [d]

[a] Tecnológico de Estudios Superiores de Ecatepec (TESE), División de Ingeniería Mecánica, Mecatrónica e Industrial, Av. Tecnológico S/N, Col. Valle de Anáhuac, C.P. 55210 Ecatepec de Morelos, Estado de México, Mexico
[b] Instituto de Investigaciones en Materiales, Unidad Morelia, Universidad Nacional Autónoma de México (UNAM), Antigua Carretera a Pátzcuaro No. 8701, Col. Ex Hacienda de San José de la Huerta, C.P. 58190 Morelia, Michoacán, Mexico
[c] Escuela Nacional de Estudios Superiores (ENES), Unidad Morelia, Universidad Nacional Autónoma de México (UNAM), Antigua Carretera a Pátzcuaro No. 8701, Col. Ex Hacienda de San José de la Huerta, C.P. 58190 Morelia, Michoacán, Mexico
[d] Laboratorio de Innovación y Evaluación en Bioenergía (LINEB) y Grupo de Innovación Ecotecnológica y Bioenergía (GIEB), Instituto de Investigaciones en Ecosistemas y Sustentabilidad (IIES), Universidad Nacional Autónoma de México (UNAM), Antigua Carretera a Pátzcuaro No. 8701, Col. Ex Hacienda de San José de la Huerta, C.P. 58190 Morelia, Michoacán, Mexico

ARTICLE INFO

Article history:
Received 11 November 2021
Revised 16 August 2022
Accepted 15 September 2022
Available online xxxx

Keywords:
Plancha-type cookstove
CFD
Thermographic images
Combustion
Modified combustion efficiency
Thermal efficiency

ABSTRACT

In this work, the performance of a biomass plancha-type cookstove in terms of thermal and modified combustion efficiencies is presented. The analysis was carried out both from a numerical and experimental point of view. To simulate the fluid flow, heat transfer, and combustion phenomena, the numerical solution of mass, momentum, thermal energy, and chemical species conservation equations was implemented in the ANSYS Fluent™ software. In particular, two domains were considered: the internal (air) volume and the metallic (solid) comal (griddle cooking surface). Additionally, a set of experiments was specially designed to measure the temperature distributions on the comal and emissions through the chimney. Three different firepower values were experimentally evaluated: 3.78, 4.72, and 5.79 kW, and they were also numerically replicated. One of the key findings of this paper is the good comparison between the thermographic images and the numerical temperature distributions for the comal surface, a difference of 24 % and 18 % for both maximum and average temperatures, respectively, is found; whereas, differences for the CO_2 mass flow rates are in the range of 1 to 27 %. The good agreements validate the correct implementation of the CFD and experimental methodologies that we have developed for the evaluation of biomass plancha-type cookstoves.

Introduction

Improved biomass stoves (IBS) may be considered efficient and sustainable technologies when they reduce GHGs that cause climate change and improve local environments (Pattanayak et al., 2019). IBS have also been proved to decrease indoor air pollution (IAP), time and cost for obtaining fuel, and to reduce deforestation (Kshirsagar & Kalamkar, 2014). In order to increase both thermal and combustion efficiencies, IBS have undergone a series of design improvements from their original models. For instance, rocket stoves have been tested using some design variations: insulation (Agenbroad et al., 2011), a drip pan pot support over the insulated rocket elbow (Agenbroad et al., 2015), the placement of a central baffle and secondary air entrainment (Pundle et al., 2019), a hybrid prototype with an inlet for primary and secondary air supplies and two combustion chambers (Kshirsagar & Kalamkar, 2020).

In the context of the plancha-type (with flat griddle cooking surface), the Patsari stove model has been changed in design over the last years. The original model (made of brick and cement) has been composed of one main combustion chamber and three circular metallic comals. It has been tested in several studies showing significant benefits (relative to traditional open fires) such as emissions reduction (Johnson et al., 2008; Medina et al., 2017a; Medina et al., 2017b; Ruiz-García et al., 2018), fuelwood savings (Berrueta et al., 2008; Masera et al., 2005), and improvements of the indoor air quality (Armendáriz-Arnez et al., 2010). In this regard, the ONIL plancha-type cookstove (now called TUYA) was also modified in order to improve its design compared with the original model, which can be seen in Jetter et al. (2012). The main modifications are in the combustion chamber which is bigger to hold more fuelwood. Furthermore, the inside ceramic parts and insulation sand form a

* Corresponding author.
E-mail address: albem@materiales.unam.mx (A. Beltrán).
[1] Present address: Tecnológico de Estudios Superiores de Ecatepec (TESE), División de Ingeniería Mecánica, Mecatrónica e Industrial, Av. Tecnológico S/N, Col. Valle de Anáhuac, C.P. 55210 Ecatepec de Morelos, Estado de México, México.

https://doi.org/10.1016/j.esd.2022.09.019
0973-0826/

ramp that transports the hot gases from the interior of the combustion chamber to the chimney. Two extra surfaces on the lateral sides of the comal were also added, they are useful to place cooking pots or pans.

Fig. 1a shows the 3D geometry and main components for the TUYA cookstove: 1) a steel comal with a thickness of 3.175 mm, 2) the combustion chamber made of mud brick and insulated with sand/gravel material, and 3) a metallic chimney to release the combustion gases. Fig. 1b shows the internal volume in which air inlet, injector, comal (plancha), and chimney's outlet are the most important geometric features for the simulations. The main dimensions of the internal volume are: the total height of the cookstove, $Z_{stove} = 1295$ mm, the chimney's internal diameter, $D_{ch} = 99.07$ mm, and its height, $Z_{ch} = 1137$ mm. The height and width of the combustion chamber entrance are $Z_{inlet} = 115$ mm and $W_{inlet} = 242$ mm, respectively. Finally, the length of the comal is $L_{comal} = 765$ mm.

Recently, computational fluid dynamics (CFD) has been used to simulate IBS and other biomass combustion devices. For instance, Chaney et al. (2012) investigated the optimization of the combustion performance and NO_X emissions of a 50 kW biomass pellet boiler. Kalla et al. (2015) reproduced the physical and chemical phenomena taking place in a natural draft wood log cookstove for low power. A review of the current state of numerical modeling of small biomass cookstoves was reported MacCarty and Bryden (2015). In the work by Silva et al. (2017), a CFD model for the combustion of the volatile gases released from biomass combustion on a grate was carried out. Mätzing et al. (2018) reported a 1D reactor cascade model to simulate the combustion of biomass and low-rank fuels in laboratory scale fixed beds. Pundle et al. (2019) presented a 2D axisymmetric steady-state CFD model of a biomass-burning natural-draft rocket cookstove. Gómez et al. (2019) presented an efficient model to simulate and analyze the steady operation and thermal behavior of biomass boilers under different working scenarios. Husain et al. (2019) carried out CFD simulations for a wide range of air velocities to predict the roles of primary and secondary airflow inside a biomass cookstove. In the work by Husain et al. (2020), a model was developed to include the spatial heterogeneity for the combustion of wood volatiles in the presence of oxygen inside a biomass cookstove. Recently, Núnez et al. (2020) studied the fluid flow, heat transfer, and gas-phase chemical reactions for a natural-draft plancha-type biomass cookstove at steady-state. A detailed CFD model for transient wood log combustion in cookstoves was developed by Scharler et al. (2020). All previous studies show an important advance in the simulation of different combustion devices; however, the comparison between experimental measurements and CFD calculations remains little explored.

In this paper, a numerical study for the transport phenomena in the TUYA plancha-type biomass cookstove is developed. It is based on the solution of mass, momentum, thermal energy, and chemical species conservation equations using the ANSYS Fluent^{TR} software. To validate the simulations, the cookstove performance was experimentally evaluated. Our measurements were focused: 1) to evaluate the energy performance parameters such as thermal efficiency and firepower, 2) to determine the emissions of carbon dioxide (CO_2), carbon monoxide (CO), and nitrogen oxides (NO_X), and 3) to obtain thermographic images for the comal. Note that this methodology is different from the one used in the standard water boiling test (WBT) (Medina et al., 2017a). All the measurements were used as a baseline to make a comparison with the numerical results. In particular, the temperature distributions on the comal obtained with the thermographic images and from the numerical simulations were compared. To the best of our knowledge, such a detailed comparison between experimental and numerical results for a biomass plancha-type cookstove has not been previously reported.

Experimental methodology

The TUYA plancha-type cookstove was evaluated with a test that consists of three replicates of 40 min each. The objective of this methodology was to reach a steady-state behavior for the transport phenomena taking place in the cookstove. It was achieved by having 10 min for stabilization and then 30 min of operating. From the experimental measurements, we neglect the first 10 min to avoid the transient-state conditions. Therefore, results are presented for the last 30 min assuming a steady-state behavior. By making an analogy with the well-known WBT methodology, the performance evaluation of the cookstove would correspond to the high power phase with a cold-start. For each test, measurements for the emissions through the chimney and temperature on the comal were performed.

Fuel

White oak (*Quercus* spp.) was used to perform all the tests with average moisture content on a wet basis of 8.5 ± 0.2% measured using a Protimeter Timbermaster Wood Moisture Meter (GE, Billerica, MA).

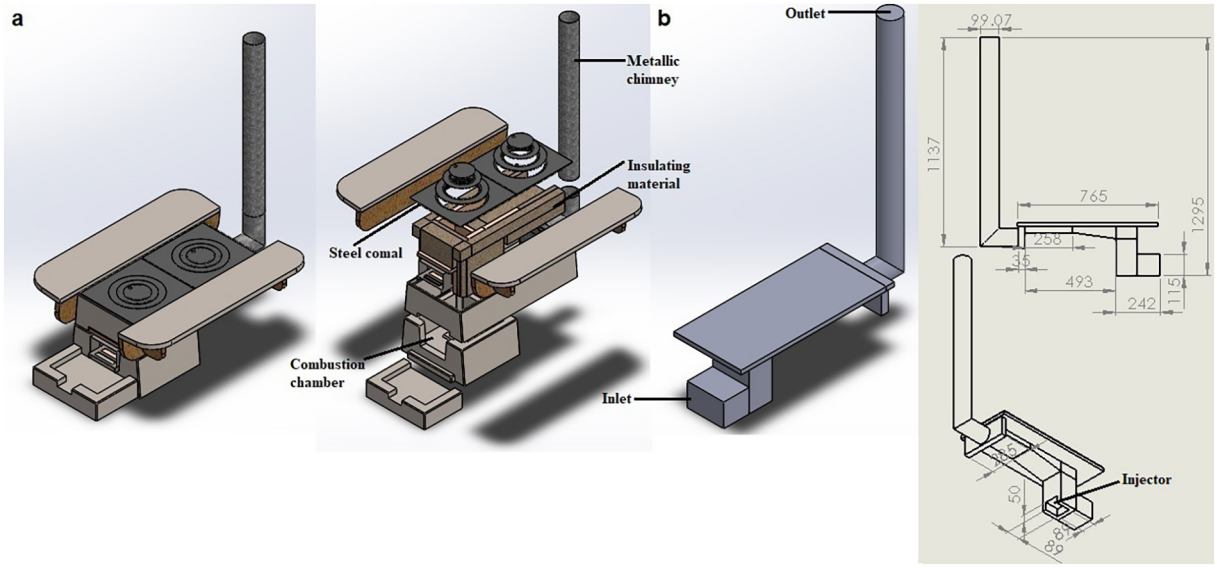

Fig. 1. (a) TUYA cookstove: Isometric external and exploded views. (b) Isometric, bottom, and lateral views of internal volume with main dimensions in mm.

Firepower evaluation

The firepower can be defined as the energy released per time by wood combustion. It is calculated according with the following equation:

$$firepower = \frac{DWC \times LHV}{Time}, \quad (1)$$

where *DWC* is the dry wood equivalent consumed (*DWC* values are given in Supplementary material), *LHV* is the lower heating value which corresponds to 17.595 MJ/kg for white oak, and the total time of each test is 40 min.

In particular, experimental tests were performed for three different firepower values: 3.78 kW (Test 1), 4.72 kW (Test 2), and 5.79 kW (Test 3). To validate our numerical methodology, simulations were run for these three firepower values, and results were compared with temperature and emissions measurements.

Temperature measurements

The temperature distribution on the comal was measured using a FLUKE^{TR} thermal camera model Ti400 which was calibrated previously. It records thermographic images of the comal when the cookstove is being operated. Measurements were recorded every minute. The temperature was checked before each test with a thermometer FLUKE^{TR} 54-II and a type K thermocouple.

Emissions measurements

Measurements of nitrogen oxides (NO_X) emissions were performed using a TESTO 340 (TESTO SE & Co, USA); whereas, for carbon dioxide (CO_2) and carbon monoxide (CO) emissions, a Q-Trak (Model 7575, TSI Inc.) was used. Emission samples were drawn through a short diameter probe inserted into the center of the flue. Real-time concentrations were measured using a non-dispersive infrared (NDIR) sensor for CO_2 and an electrochemical cell to measure CO and NO_X. CO_2 and CO sensors were calibrated using zero air and a mixture of 500 ppm of CO and 5000 ppm of CO_2. NO_X sensor was calibrated by TESTO SE & Co.

Numerical methodology

A hexahedral mesh was built with a high spatial resolution near the interior surfaces of the geometry and the volatiles' injection zone, see Fig. 2.

A total of 633,910 elements were used (see the Grid sensitivity study section). Some average mesh parameters are the skewness and orthogonal quality equal to 0.11 and 0.93, respectively.

Mass flow rate of wood volatiles

The following chemical reaction was considered for the biomass combustion where the elemental molar composition of wood volatiles is (Medina et al., 2021; Núnez et al., 2020):

$$CH_{2.116}O_{1.075} + 1.058\,O_2 \rightarrow CO_2 + 1.191\,H_2O$$

The *DWC* and the total time for each test were taken into account to estimate the inlet mass flow rate of wood volatiles. The results were 2.54×10^{-4} kg/s, 3.30×10^{-4} kg/s, and 3.68×10^{-4} kg/s for the Tests 1, 2, and 3, respectively; whereas, the oxygen required to burn the biomass was estimated by taking account the previous flows and the stoichiometry of the reaction. In addition, an excess oxygen ratio of 2 was considered to ensure a sufficient mixing O_2/wood volatiles as suggested by Koppejan and Van Loo (2012). The values were 5.49×10^{-4} kgO_2/s, 7.13×10^{-4} kgO_2/s, and 7.96×10^{-4} kgO_2/s for the Tests 1, 2, and 3, respectively. For a more detailed explanation, see Supplementary material.

Discrete ordinates (DO) radiation model

Heat transfer processes (conduction, convection, and radiation) are important phenomena in cookstoves (Kumar et al., 2013). In our simulations, the conduction phenomenon takes place on the comal (solid) domain; whereas convection occurs due to the buoyancy force, and in the convective cooling of the surfaces of the cookstove (boundary conditions). The radiation phenomenon is the most important mechanism to transfer heat in high temperature systems such as cookstoves devices (Gómez et al., 2019). To simulate the radiation in the overall computational domain, the discrete ordinates (DO) model was chosen. Its use is as also reported by Karim and Naser (2018), Somwangthanaroj and Fukuda (2020), and Tu et al. (2019). The entire details for this model can be seen in the ANSYS Fluent user's guide (*ANSYS fluent theory guide*, 2013).

Finally, boundary conditions were imposed on the six different zones created on the geometry of the internal volume: chimney, comal, inlet, outlet, injector, and wall (rest of the body). The inlet zone is assumed as the air entrance. An ambient temperature (T_∞) of 298 K was fixed. It should be pointed out that, the inlet mass flow rates were imposed as a boundary condition on the injector zone with an initial temperature of 1473 K according with adiabatic combustion temperature for an excess oxygen ratio of 2 (Koppejan & Van Loo, 2012). This zone is located inside the combustion chamber with width, length, and depth dimensions of 50, 89, and 89 mm, respectively, see Fig. 1b. Depending on the firepower value to be simulated, final temperature values at the injection zone were 1000 and 1275 K, which are in the range of the expected values as reported in the literature (Kumar et al., 2013;

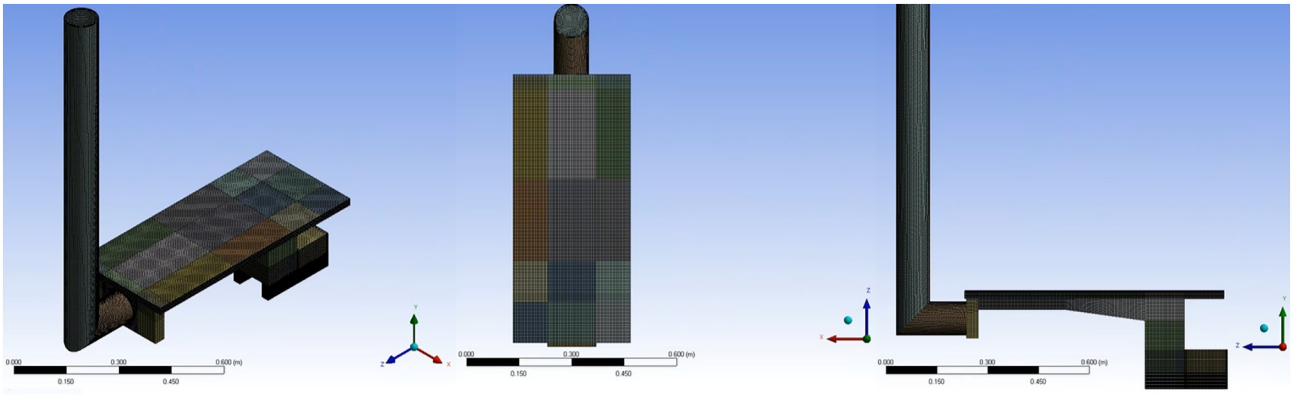

Fig. 2. Hexahedral mesh for TUYA plancha-cookstove. From left to right: Isometric, top, and lateral views.

Table 1
Grid sensitivity study for the average temperature.

Elements	T_{ave} (K)	% difference
1,233,599	462.42	4.3
633,910	442.69	–
515,408	462.73	4.3
351,704	463.34	4.5

Núnez et al., 2020). Based on the inlet mass flow rate and the temperature values, the firepower values reached in the simulations were 3.77, 4.73, and 5.73 kW for Tests 1, 2, and 3, respectively. Due to the high temperature and the interaction with the oxygen flow coming from the inlet, the combustion process starts, see the work reported by Núnez et al. (2020).

For the chimney zone, thermal properties for the steel (fabrication material), a wall thickness of 1 mm, and a convective heat transfer coefficient of $h = 40\ \mathrm{W/m^2\ K}$ were used. The same h value was used for the comal zone, it is quite similar to the one used in other works (MacCarty & Bryden, 2016; Prapas, 2007). At the outlet zone, the temperature was fixed to 373 K (Medina et al., 2017a) and the mole fraction of CO_2 was 46 % according to the stoichiometric calculations. For the rest of the walls (identified as wall zone) an adiabatic condition was assumed. For the simulations, a user-defined function (UDF) was developed that computes O_2 - N_2 temperature mass diffusivity, used in the wood volatile mixture.

Global parameters

For the evaluation of the performance of the cookstove, the thermal (Núnez et al., 2020) and modified combustion (Scharler et al., 2009) efficiencies are useful parameters.

The thermal efficiency is defined as:

$$\eta = \frac{\dot{Q}_p}{firepower}, \tag{2}$$

where $\dot{Q}_p$ is the average rate of heat transfer through the comal.

$\dot{Q}_p$ can be directly obtained from the simulations and for the experiments, it is calculated as:

$$\dot{Q}_p = mC_p(T_{\max} - T_\infty), \tag{3}$$

where m is the mass of the comal and C_p is the specific heat capacity of the comal's fabrication metal. For our cookstove $m = 7.813$ kg and $C_p = 486\ \mathrm{J/kg\ K}$. T_{max} is the maximum temperature of the comal, which can be obtained from the thermographic images, see the Comal temperature distribution section.

The unburned volatile combustion efficiency (UVE) is calculated as (Medina et al., 2021):

$$UVE = \frac{\dot{m}_{CO_2}}{\dot{m}_{CO_2} + \dot{m}_{WV}}, \tag{4}$$

where WV stands for unburned wood volatiles at the exit of the chimney.

As can be seen from previous equations, η is defined as the ratio of the average rate of heat release on the comal and the firepower; whereas, the UVE parameter is defined as the ratio of CO_2 mass flow rate ($\dot{m}_{CO_2}$) and the sum of mass flow rates for CO_2 and wood volatiles ($\dot{m}_{WV}$), both evaluated at the outlet boundary condition.

Grid sensitivity study

For the grid sensitivity analysis, the average temperature on the comal, T_{ave}, is measured for four different grids and for a firepower of 5.73 kW. Table 1 shows that T_{ave} changes no more than 4.5 % with respect to the grid with 633,910 elements, the one used in all calculations.

Results and discussion

To keep the presentation of the results brief, a comparison between temperature isocontours obtained from the simulations and thermographic images for the comal, as well as temperature profiles for the comal's centerline (in the axial direction), are presented. At the end of the section, experimental measurements for the mass flow rates of $CO_2\ (\dot{m}_{CO_2})$, CO $(\dot{m}_{CO})$, and $NO_X\ \left(\dot{m}_{NO_X}\right)$ are presented. Finally, thermal and modified combustion efficiencies are summarized for each firepower value.

Comal temperature distribution

Fig. 3 shows the experimental data for T_{ave}. Values were extracted from the thermographic images. As can be seen, while Tests 1 and 3 report a steady state, the temperature in Test 2 was increasing as a function of time. Despite some time variations, a steady-state behavior for the average temperature values can be assumed.

Fig. 4 shows comparisons for the temperature isocontours obtained from the simulations and the ones measured by the thermographic camera. Interestingly, from the experimental and numerical results, it can be seen that the highest temperatures are concentrated in the comal region located above the combustion chamber. Temperature isocontours exhibit

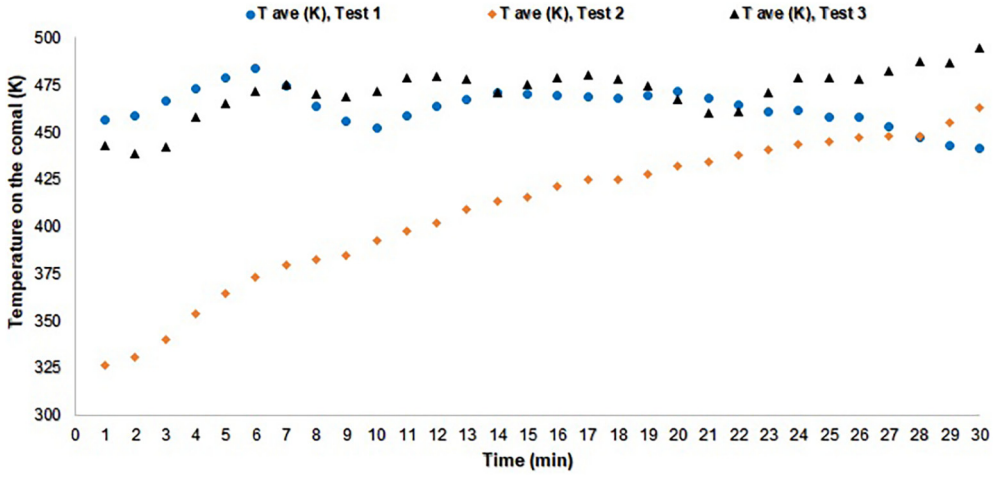

Fig. 3. Average experimental temperatures on the comal vs. Time.

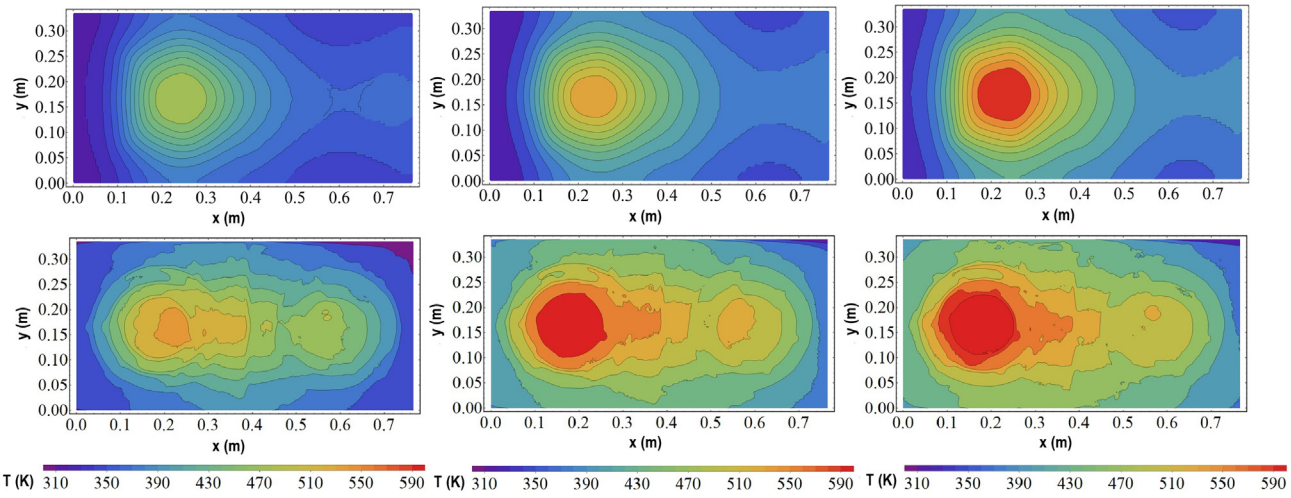

Fig. 4. Average temperature isocontours on the comal over the total time. Top and bottom rows correspond to numerical results and thermographic images, respectively. From the left to the right experimental firepower values are 3.78, 4.72, and 5.79 kW; whereas, simulations correspond to 3.77, 4.73, and 5.73 kW. Color bars indicate the temperature.

a circular shape elongated in the direction of the chimney. The chimney (not shown) is located on the right side of the images. In addition, the relationship between firepower and temperature is clear in Test 3, where for the highest firepower the highest temperature is reported.

For a more detailed comparison between experimental and numerical results, Fig. 5 shows the temperature on the comal as a function of the axial centerline. The experimental measurements reach the highest temperatures in the first zone of the axial center plane close to the region of the combustion chamber; whereas, for the numerical results, these temperatures were also found near the first zone. This behavior can be explained as a result of the area of the injection zone used in the simulations, which is significantly different from the complex distribution of the wood-logs in the combustion chamber. Despite the differences the order of magnitude and profiles shape are well reproduced by the simulations.

In addition, Table 2 reports the comparison between average and maximum temperatures on the comal for experimental measurements and numerical simulations. Differences are in the range of 14 to 18 %, and 10 to 24 % for average and maximum temperatures, respectively. Other related studies report differences in the same range; for instance, 3 to 12 % and 1 to 34 % in the works by Kalla et al. (2015) and Scharler et al. (2009), respectively.

The highest (experimental and numerical) temperature values were obtained for Test 3. A similar result was found by Pande et al. (2019) where they report a relationship between larger firepower values and bigger flame propagation.

Temperature and velocity patterns in the axial plane

Based on the 3D numerical simulations, it is possible to model the temperature and the flow behaviors inside the cookstove. Fig. 6 shows the temperature and the velocity isocontours in the axial plane of the cookstove. As expected, the highest temperature is located above the injection zone, in the center of the combustion chamber region, and the surrounding hot air transfers the heat to the comal during its trajectory to the exit of the chimney. The highest velocities values are reached near the base of the chimney.

It should be pointed out that previous studies have reported the temperature distribution of different biomass combustion devices by using CFD tools (Gómez et al., 2019; Karim & Naser, 2018; Scharler et al., 2009; Silva et al., 2017; Somwangthanaroj & Fukuda, 2020). However, the good comparison between thermographic images and simulations here presented is an important advance in CFD studies for biomass plancha-type cookstoves. In this regard, the shape similarities of the temperature distribution on the comal for the three tests (see, Fig. 4) show that the transport phenomena are correctly simulated.

Emissions measurements

Fig. 7 shows the time evolution of CO_2 mass flow rate and the *UVE* parameters for the three experimental tests. Results show that CO_2 emissions are linked with the *UVE*, which has been reported in other

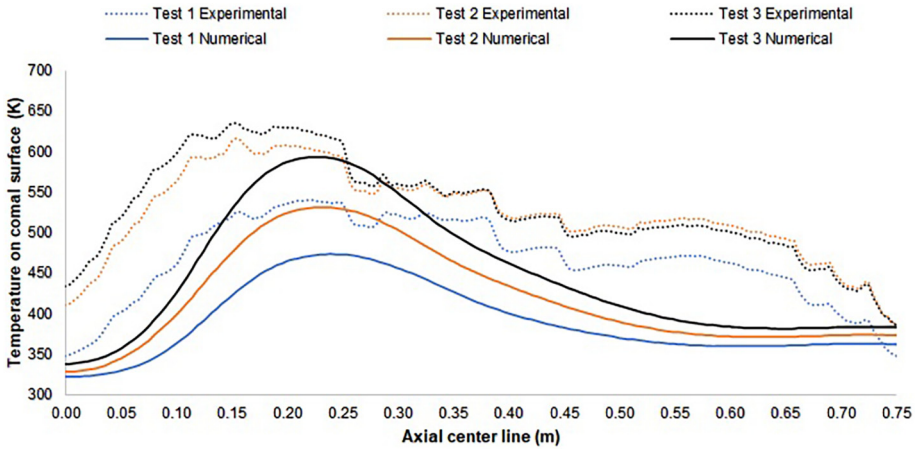

Fig. 5. Experimental and numerical temperature profiles along the axial centerline of the surface of the comal.

Table 2
Experimental and numerical results for the average and maximum temperatures on the comal.

Test	1	2	3
Comal temperature	T_{ave} (K)	T_{ave} (K)	T_{ave} (K)
Experimental	458.47 ± 47.54	508.36 ± 46.56	514.35 ± 48.77
Numerical	387.69 ± 30.93	416.12 ± 41.69	442.69 ± 52.73
% difference	15	18	14

Test	1	2	3
Comal temperature	T_{max} (K)	T_{max} (K)	T_{max} (K)
Experimental	529.07	584.63	594.10
Numerical	441.19	443.27	534.01
% difference	17	24	10

works (Johnson et al., 2010; Medina et al., 2017a; Medina et al., 2017b). However, *UVE* can decrease when the stove is overloaded (Medina et al., 2017a). Results also show the relationship between the combustion efficiency and the emission of the products of the incomplete combustion. As can be seen in Fig. 8, when *UVE* decreases, CO and NO_X present significant emission peaks in Tests 1 and 3. Low CO and NO_X emission rates were observed in Test 2, which is an indication of a better combustion process.

CO emissions have been reported, such as one of the main gases of an inefficient combustion process in cookstoves (Jetter et al., 2012; Jetter & Kariher, 2009; Johnson et al., 2010; MacCarty et al., 2008; Roden et al., 2009). On the other hand, the NO_X emissions are formed because of the nitrogen content in the biomass as reported by Deng et al. (2018). Furthermore, these emissions tend to increase with higher combustion temperatures, and the nitrogen conversion to NO_X can be close to 100 % (Koppejan & Van Loo, 2012).

Energy and emissions performance

A detailed comparison between experimental and numerical results for the CO_2 mass flow rate, the firepower, the thermal efficiency, and the *UVE* can be seen in Table 3. The largest differences for the thermal efficiency and CO_2 mass flow rate are observed in Test 2 with values of 51 % and 27 %, respectively. Differences for the firepower are very small (1 %), and for the *UVE* are in the range of 2 to 5 %.

Although it is well known that the rate of pollutant emissions changes over time, the good comparison between experimental and numerical results for the CO_2 mass flow rate is an indication that the assumption of steady-state behavior for the cookstove performance is not far from reality.

The CO_2 mass flow rates had an average difference of 18 % between experimental and numerical results. Nevertheless, the

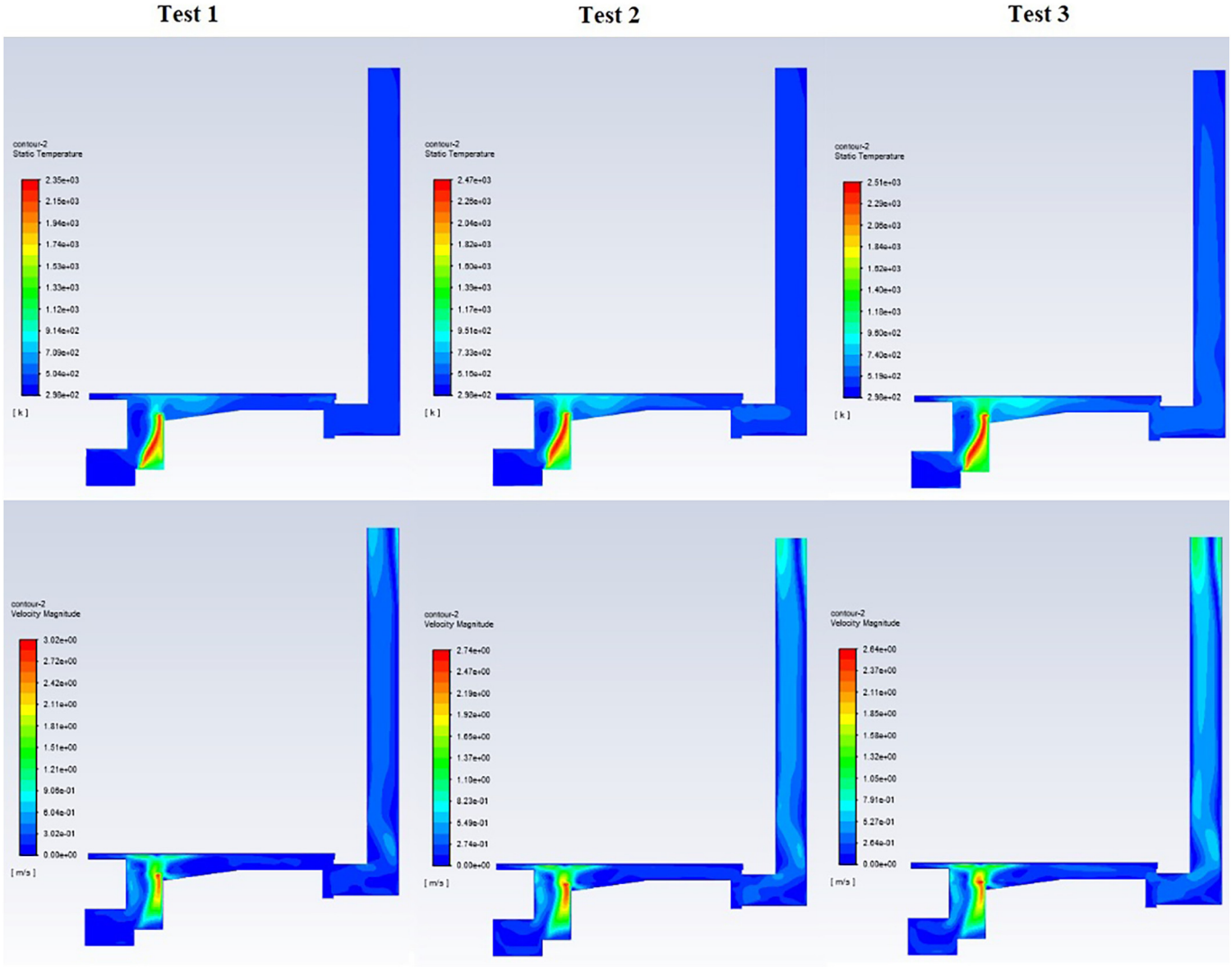

Fig. 6. Temperature (top row) and velocity (bottom row) isocontours in the axial plane. Color bars indicate either temperature or velocity magnitude.

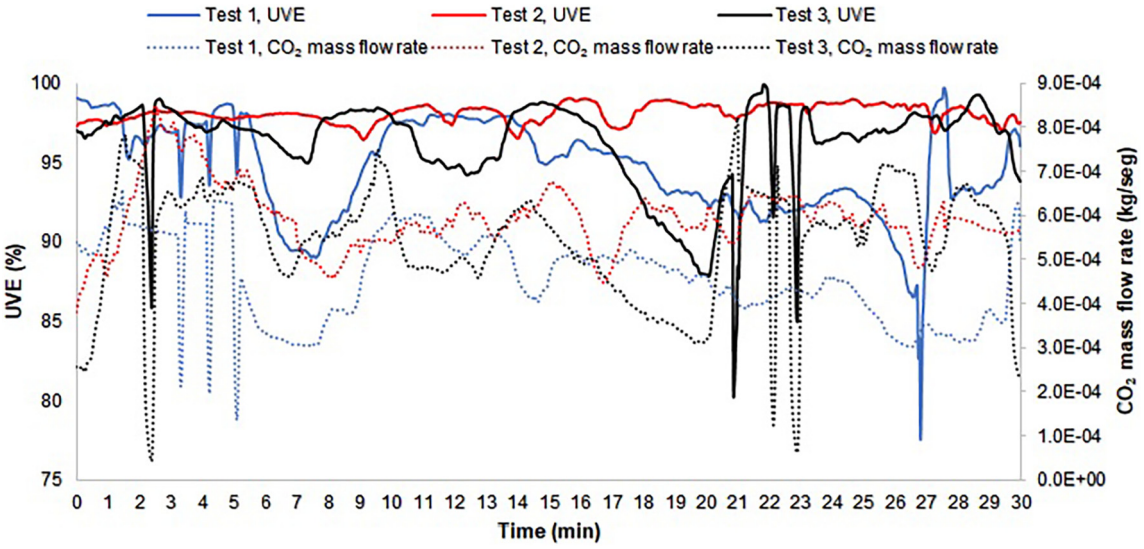

Fig. 7. Time evolution of *UVE* and CO_2 mass flow rate for the experimental tests.

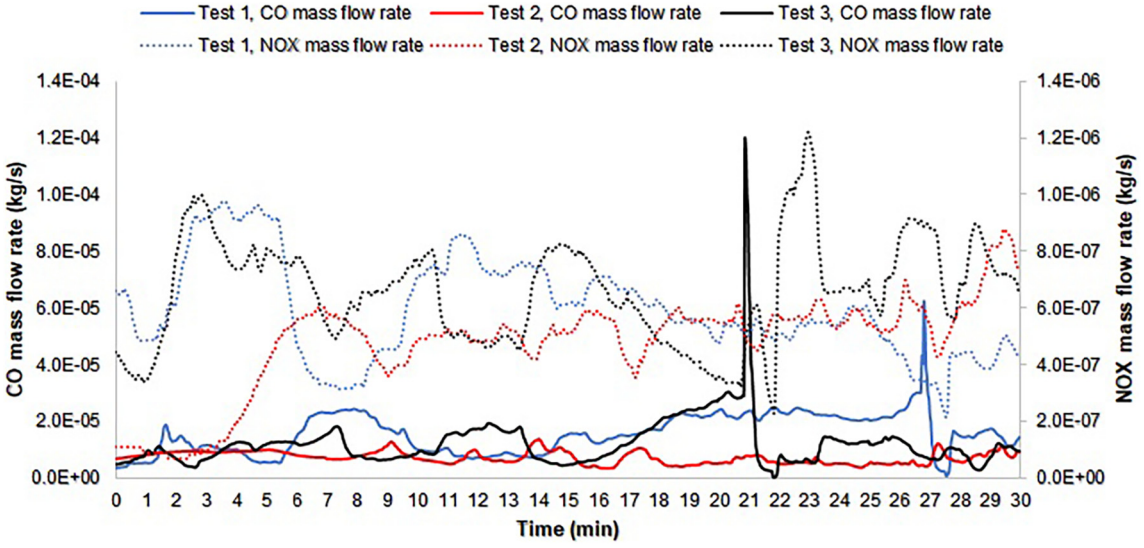

Fig. 8. Time evolution of CO and NO_X emission rates for the experimental tests.

stoichiometric calculations (see, Supplementary material) obtain the following results: 3.57×10^{-4} kg/s, 4.63×10^{-4} kg/s, and 5.15×10^{-4} kg/s for Tests 1, 2, and 3, respectively. By comparing with the simulated CO_2 mass flow rate values, the differences were up to 6 %, which is an indication of the correct chemical assumptions, such as excess oxygen ratio, in the numerical simulations. Similar studies have found an emissions discrepancy of up to 100 % (Miller-Lionberg, 2011). The comparison for *UVE* showed also a good agreement with a major difference of 5 %, which validates the correct assumption in Eq. (4). On the other hand, significant differences in thermal efficiencies were found for the three tests. It might be attributed to smaller experimental values for the $(T_{max} - T_{\infty})$ difference due to oxide on the bottom face (the one in direct contact with the flames) of the comal.

Table 3
Comparison between experimental and numerical results for some global parameters.

Experimental/numerical	Test	$\dot{m}_{CO_2}$ (kg CO_2/s)	Firepower (kW)	η (%)	*UVE* (%)
Experimental	1	$4.58 \times 10^{-4} \pm 9.67 \times 10^{-5}$	3.78	16.01	94.58 ± 3.03
Numerical	1	3.41×10^{-4}	3.77	20.30	99.91
% difference	–	26	1	21	5
Experimental	2	$5.96 \times 10^{-4} \pm 7.47 \times 10^{-5}$	4.72	10.33	98.11 ± 0.56
Numerical	2	4.33×10^{-4}	4.73	20.88	99.93
% difference	–	27	1	51	2
Experimental	3	$5.43 \times 10^{-4} \pm 1.32 \times 10^{-4}$	5.79	10.77	96.22 ± 2.73
Numerical	3	5.44×10^{-4}	5.73	21.32	99.95
% difference	–	1	1	49	4

Conclusions

This study provides a comprehensive assessment of a direct comparison between experimental and numerical results for the evaluation of a biomass plancha-type cookstove. Below are some of the key findings:

- Even though some fluctuations in the measurements were observed, a steady-state behavior for the experiments can be assumed.
- The shape similarities of the temperature distribution on the comal for the three tests show that the transport phenomena are correctly simulated.
- The relationship between UVE and pollutant emissions was found to be clear. When UVE decreases, products of incomplete combustion such as CO and NO_X are significantly produced, see Tests 1 and 3. UVE can be reduced when the airflow is restricted by overfeeding fuel into the combustion chamber.
- For the heat transfer in the stove, there are some important consideration that should be noted: 1) The radiation model was considered only in the combustion chamber geometry. 2) The radiation from the comal to the ambient is not considered. A convective boundary condition is used on the comal surface. 3) The experimental tests were performed without food/pots over the comal surface.
- Other cookstove devices can be easily evaluated using the experimental and numerical methodologies here presented.

Finally, it should be pointed out that the influence of the tester, fuel properties, size sample of the experimental tests, and operation of the cookstove itself are key variables in the global performance (emissions and energy). They can help to explain the differences found between experimental and numerical results.

Declaration of competing interest

Authors wish to confirm that there are no known conflicts of interest associated with this publication and there has been no significant financial support for this work that could have influenced its outcome.

Acknowledgements

Authors would like to acknowledge SENER-CONACyT 2014-246911 Clúster de Biocombustibles Sólidos para la Generación Térmica y Eléctrica for financial support. Paulo Medina would like to thank Consejo Nacional de Ciencia y Tecnología (CONACyT) for the Posdoctoral Fellowship 741045 2019-2020 at IIM-UNAM and to the Sistema Nacional de Investigadores (SNI) for the current designation and support CVU 373288 Request 346259. CFD computations and experimental measurements were performed at the Laboratory for Design, Modeling, and Simulations (LDMS) at the Morelia Unit of the IIM-UNAM and the Laboratorio de Innovación y Evaluación de Estufas de Biomasa (LINEB) at IIES-UNAM, respectively. Authors thank Gibran Aguilasocho-Acosta and Saúl Villareal for their help and support with the meshing activities. Authors also thank Alejandro Pompa and Alberto López-Vivas† for the HPC support.

Appendix A. Supplementary data

Supplementary data to this article can be found online at https://doi.org/10.1016/j.esd.2022.09.019.

References

ANSYS fluent theory guide. (2013).275 Technology Drive Canonsburg, PA 15317: ANSYS Inc.

Agenbroad, J., DeFoort, M., Kirkpatrick, A., & Kreutzer, C. (2011). A simplified model for understanding natural convection driven biomass cooking stoves—Part 1: Setup and baseline validation. *Energy for Sustainable Development*, *15*(2), 160–168.

Agenbroad, J., DeFoort, M., Kirkpatrick, A., & Kreutzer, C. (2015). A simplified model for understanding natural convection driven biomass cooking stoves—Part 2: with cook piece operation and the dimensionless form. *Energy for Sustainable Development*, *15*(2), 169–175.

Armendáriz-Arnez, C., Edwards, R. D., Johnson, M., Rosas, I. A., Espinosa, F., & Masera, O. R. (2010). Indoor particle size distributions in homes with open fires and improved patsari cook stoves. *Atmospheric Environment*, *44*(24), 2881–2886.

Berrueta, V. M., Edwards, R. D., & Masera, O. R. (2008). Energy performance of wood-burning cookstoves in Michoacán, Mexico. *Renewable Energy*, *33*(5), 859–870.

Chaney, J., Liu, H., & Li, J. (2012). An overview of cfd modelling of small-scale fixed-bed biomass pellet boilers with preliminary results from a simplified approach. *Energy Conversion and Management*, *63*, 149–156.

Deng, L., Torres-Rojas, D., Burford, M., Whitlow, T. H., Lehmann, J., & Fisher, E. M. (2018). Fuel sensitivity of biomass cookstove performance. *Applied Energy*, *215*, 13–20.

Gómez, M., Martín, R., Chapela, S., & Porteiro, J. (2019). Steady cfd combustion modeling for biomass boilers: An application to the study of the exhaust gas recirculation performance. *Energy Conversion and Management*, *179*, 91–103.

Husain, Z., Tiwari, S. S., Kataria, A., Mathpati, C. S., Pandit, A. B., & Joshi, J. B. (2020). Computational fluid dynamic study of biomass cook stove—Part 2: Devolatilization and heterogeneous combustion. *Industrial & Engineering Chemistry Research*, *59*(32), 14507–14521.

Husain, Z., Tiwari, S. S., Pandit, A. B., & Joshi, J. B. (2019). Computational fluid dynamics study of biomass cook stove—Part 1: Hydrodynamics and homogeneous combustion. *Industrial & Engineering Chemistry Research*, *59*(9), 4161–4176.

Jetter, J., Zhao, Y., Smith, K. R., Khan, B., Yelverton, T., DeCarlo, P., et al. (2012). Pollutant emissions and energy efficiency under controlled conditions for household biomass cookstoves and implications for metrics useful in setting international test standards. *Environmental Science & Technology*, *46*(19), 10827–10834.

Jetter, J. J., & Kariher, P. (2009). Solid-fuel household cook stoves: characterization of performance and emissions. *Biomass and Bioenergy*, *33*(2), 294–305.

Johnson, M., Edwards, R., Berrueta, V., & Masera, O. (2010). New approaches to performance testing of improved cookstoves. *Environmental Science & Technology*, *44*(1), 368–374.

Johnson, M., Edwards, R., Frenk, C. A., & Masera, O. (2008). In-field greenhouse gas emissions from cookstoves in rural Mexican households. *Atmospheric Environment*, *42*(6), 1206–1222.

Kalla, S., Marcoux, H., & deChamplain, A. (2015). Cfd approach for modelling high and low combustion in a natural draft residential wood log stove. *International Journal of Heat and Technology*, *33*(1), 33–38.

Karim, M. R., & Naser, J. (2018). Cfd modelling of combustion and associated emission of wet woody biomass in a 4 mw moving grate boiler. *Fuel*, *222*, 656–674.

Koppejan, J., & Van Loo, S. (2012). *The handbook of biomass combustion and co-firing.* Routledge.

Kshirsagar, M. P., & Kalamkar, V. R. (2014). A comprehensive review on biomass cookstoves and a systematic approach for modern cookstove design. *Renewable and Sustainable Energy Reviews*, *30*, 580–603.

Kshirsagar, M. P., & Kalamkar, V. R. (2020). Application of multi-response robust parameter design for performance optimization of a hybrid draft biomass cook stove. *Renewable Energy*, *153*, 1127–1139.

Kumar, M., Kumar, S., & Tyagi, S. (2013). Design, development and technological advancement in the biomass cookstoves: a review. *Renewable and Sustainable Energy Reviews*, *26*, 265–285.

MacCarty, N., Ogle, D., Still, D., Bond, T., & Roden, C. (2008). A laboratory comparison of the global warming impact of five major types of biomass cooking stoves. *Energy for Sustainable Development*, *12*(2), 56–65.

MacCarty, N. A., & Bryden, K. M. (2015). Modeling of household biomass cookstoves: A review. *Energy for Sustainable Development*, *26*, 1–13.

MacCarty, N. A., & Bryden, K. M. (2016). A generalized heat-transfer model for shielded-fire household cookstoves. *Energy for Sustainable Development*, *33*, 96–107. https://doi.org/10.1016/j.esd.2016.03.003.

Masera, O. R., Díaz, R., & Berrueta, V. (2005). From cookstoves to cooking systems: The integrated program on sustainable household energy use in Mexico. *Energy for Sustainable Development*, *9*(1), 25–36.

Mätzing, H., Gehrmann, H. J., Seifert, H., & Stapf, D. (2018). Modelling grate combustion of biomass and low rank fuels with cfd application. *Waste Management*, *78*, 686–697.

Medina, P., Berrueta, V., Martínez, M., Ruiz, V., Edwards, R., & Masera, O. (2017). Comparative performance of five Mexican plancha-type cookstoves using water boiling tests. *Development Engineering*, *2*, 20–28.

Medina, P., Berrueta, V., Martínez, M., Ruiz, V., Ruiz-Mercado, I., & Masera, O. (2017). Closing the gap between lab and field cookstove tests: Benefits of multi-pot and sequencing cooking tasks through controlled burning cycles. *Energy for Sustainable Development*, *41*, 106–111.

Medina, P., Núñez, J., Ruiz-Garcá, V. M., & Beltrán, A. (2021). Experimental and numerical comparison of co2 mass flow rate emissions, combustion and thermal performance for a biomass plancha-type cookstove. *Energy for Sustainable Development*, *63*, 153–159.

Miller-Lionberg, D. D. (2011). *A fine resolution CFD simulation approach for biomass cook stove development.* Colorado State University.

Núnez, J., Moctezuma-Sánchez, M. F., Fisher, E. M., Berrueta, V. M., Masera, O. R., & Beltrán, A. (2020). Natural-draft flow and heat transfer in a plancha-type biomass cookstove. *Renewable Energy*, *146*, 727–736.

Pande, R. R., Sharma, S. K., & Kalamkar, V. R. (2019). Experimental and numerical analyses for designing two-pot biomass cookstove. *Journal of the Brazilian Society of Mechanical Sciences and Engineering*, *41*(8), 350.

Pattanayak, S. K., Jeuland, M., Lewis, J., Usmani, F., Brooks, N., Bhojvaid, V., et al. (2019). Experimental evidence on promotion of electric and improved biomass cookstoves. *Proceedings of the National Academy of Sciences*, *116*(27), 13282–13287.

Prapas, J. (2007). *Toward the understanding and optimization of chimneys for buoyantly driven biomass stoves.* Ph.D. thesisColorado State University.

Pundle, A., Sullivan, B., Means, P., Posner, J. D., & Kramlich, J. C. (2019). Predicting and analyzing the performance of biomass-burning natural draft rocket cookstoves using computational fluid dynamics. *Biomass and Bioenergy*, *131*, Article 105402.

Roden, C. A., Bond, T. C., Conway, S., Pinel, A. B. O., MacCarty, N., & Still, D. (2009). Laboratory and field investigations of particulate and carbon monoxide emissions from traditional and improved cookstoves. *Atmospheric Environment*, *43*(6), 1170–1181.

Ruiz-García, V. M., Edwards, R. D., Ghasemian, M., Berrueta, V. M., Princevac, M., Vazquez, J. C., et al. (2018). Fugitive emissions and health implications of plancha-type stoves. *Environmental Science & Technology*, *52*(18), 10848–10855.

Scharler, R., Benesch, C., Neudeck, A., & Obernberger, I. (2009). Cfd based design and optimisation of wood log fired stoves. *Proc of 17th EU BC&E, Hamburg* (pp. 1361–1367).

Scharler, R., Gruber, T., Ehrenhöfer, A., Kelz, J., Bardar, R. M., Bauer, T., et al. (2020). Transient cfd simulation of wood log combustion in stoves. *Renewable Energy*, *145*, 651–662.

Silva, J., Teixeira, J., Teixeira, S., Preziati, S., & Cassiano, J. (2017). Cfd modeling of combustion in biomass furnace. *Energy Procedia*, *120*, 665–672.

Somwangthanaroj, S., & Fukuda, S. (2020). Cfd modeling of biomass grate combustion using a steady-state discrete particle model (dpm) approach. *Renewable Energy*, *148*, 363–373.

Tu, Y., Xu, M., Zhou, D., Wang, Q., Yang, W., & Liu, H. (2019). Cfd and kinetic modelling study of methane mild combustion in o2/n2, o2/co2 and o2/h2o atmospheres. *Applied Energy*, *240*, 1003–1013.